11-1-1994

Mean-Field Theory for Alkali-Metal-Doped Polyacetylene

A. Brooks Harris
University of Pennsylvania, harris@sas.upenn.edu

Recommended Citation

Harris, A. (1994). Mean-Field Theory for Alkali-Metal-Doped Polyacetylene. *Physical Review B, 50* (17), 12441-12457. http://dx.doi.org/10.1103/PhysRevB.50.12441

Mean-Field Theory for Alkali-Metal-Doped Polyacetylene

Abstract

The Landau theory used by Choi and Mele (CM) to treat their rotor model on a triangular lattice for the orientational ordering of polyacetylene chains in alkali-metal-doped polyacetylene is studied. A reanalysis of the higher-order terms in the Landau expansion indicates that cosine ordering can support a nonzero cubic term in the Landau expansion whereas the sine-ordered phase has no such term. To construct a phase diagram requires a numerical solution of the self-consistent equations of mean-field theory. Although this analysis does not convincingly treat the incommensurate phases found by CM, it does identify an unusually rich variety of thermodynamically stable phases and leads to significant modifications of the previous phase diagram. However, we do confirm the principle result of CM, that alkali-metal doping tends to destabilize the herringbone phase that exists in the undoped system. We also identify a number of interesting multicritical points. At one of these, the quadratic terms in the Landau expansion are totally independent of wave vector. This situation is similar to that for the *kagomé* antiferromagnet.

Disciplines

Physics

Mean-field theory for alkali-metal-doped polyacetylene

A. B. Harris
Department of Physics, University of Pennsylvania, Philadelphia, Pennsylvania 19104
(Received 5 August 1992; revised manuscript received 2 December 1992)

The Landau theory used by Choi and Mele (CM) to treat their rotor model on a triangular lattice for the orientational ordering of polyacetylene chains in alkali-metal-doped polyacetylene is studied. A reanalysis of the higher-order terms in the Landau expansion indicates that cosine ordering can support a nonzero cubic term in the Landau expansion whereas the sine-ordered phase has no such term. To construct a phase diagram requires a numerical solution of the self-consistent equations of mean-field theory. Although this analysis does not convincingly treat the incommensurate phases found by CM, it does identify an unusually rich variety of thermodynamically stable phases and leads to significant modifications of the previous phase diagram. However, we do confirm the principle result of CM, that alkali-metal doping tends to destabilize the herringbone phase that exists in the undoped system. We also identify a number of interesting multicritical points. At one of these, the quadratic terms in the Landau expansion are totally independent of wave vector. This situation is similar to that for the *kagomé* antiferromagnet.

I. INTRODUCTION

Recent experiments have established the existence of a very rich phase diagram for the crystalline polyacetylene system as a function of conentration of alkali-metal dopants (or better, in terms of the chemical potential, μ of these dopants). An interesting phenomenon in these systems is the orientational ordering of the polyacetylene chains. To discuss the ordering of such molecules we will refer to the principle axes as defined by the moment of inertia tensor of the molecule. The "long" axis lies along the chain direction. The "medium" axis is perpendicular to the long axis and lies in the plane of the molecule. The "short" axis is perpendicular to the plane of the molecule. In the crystalline systems, the long axis lies along the crystal $\underline{c}$ axis. This paper is concerned with the ordering of the medium axes in the $\underline{a}$-$\underline{b}$ or x-y plane. We consider these projections to be quadrupolar objects (thus neglecting the lack of a vertical mirror plane associated with reversing the direction of the medium axis). Henceforth we will refer to these quadrupolar projections as "rotors," and thereby do not allow the molecules to have any twist in their equilibrium configuration.

For the undoped polyacetylene,[1] a herringbonelike ordering of rotors was found, with a setting angle, ϕ, whose value was not fixed by symmetry. In contrast, the simplest rotor models[2,3] predict a true herringbone ordering with ϕ fixed by symmetry to be 45°, independent of temperature. Accordingly, as predicted[3] for polyacetylene, the ϕ angle was found[4] to be temperature dependent. This lower symmetry is also indicated by the temperature dependence of the ratio, b/a, of in-plane lattice constants which deviates from that of the perfect triangular lattice.[4]

Polyacetylene, when alkali-metal-doped, can exhibit alterations in its orientational state. In particular, even for moderate doping, the herringbone ordering is destroyed.[5,6] These results inspired an elegant, but simple, model Hamiltonian, which was shown by Choi and Mele[7] (CM) to reproduce qualitatively the structural changes due to alkali-metal-doping. This model represents a nontrivial extension of a comprehensive mean-field analysis of the pure system as described by a general model for anisotropic rotors.[3] In the CM model alkali-metal doping is assumed to occur by completely filling a number of z-directed galleries between three adjacent polyacetylene polymers. They found that upon sufficient doping, the ordered phase was one displaying combined compositional and orientational ordering. Such a phenomenon was predicted[8] [Harris, Mouritsen, and Berlinsky (HMB)] some time ago, and later observed,[9] for diluted diatomics physisorbed on a graphite substrate. The CM model for doped polyacetylene and the HMB model for randomly diluted diatomics on grafoil differ in some details. The CM model is simpler than the HMB model in that it describes rotors in a plane, characterized by a single angle θ_i, whereas the HMB model dealt with three-dimensional rotors. On the other hand, the CM model shows a richer phase diagram than the HMB model because it includes more possibilities for frustration. Thus CM found regimes in the phase diagram for the existence of incommensurate phases, either with a single wave vector or with a superposition of three wave vectors. The latter states are similar to those found previously in other contexts.[10–12] The existence and nature of these phases, as well as whether or not the ordering transition is discontinuous, depends on the form of the higher-than-quadratic terms in the Landau expansion. As we shall see, the CM treatment of these terms was not completely correct. The purpose of the present paper is the present and improved analysis of the relevant higher-order terms in Landau theory and an elucidation of the phase diagram. In fact, we find that these higher-order terms often result in a discontinuous transition. Since these

0163-1829/94/50(17)/12441(17)/$06.00

terms are not scaled by a small parameter, a Landau expansion cannot provide a controlled description of the ordering or of the resulting ordered phases. Accordingly, to construct the phase diagram we had recourse to a numerical implementation of the self-consistent equations of mean-field theory based on periodic structures with a small unit cell. Unfortunately, such a treatment does not allow us to access incommensurate phases. Therefore, in some regimes, we are not entirely certain whether or not incommensurate phases actually exist within mean field theory for this model. Nevertheless, our results do indicate the thermodynamic stability of a much richer variety of phases than hitherto suspected.

Briefly, this paper is organized as follows. In Sec. II we record the general form of the Landau expansion and develop explicit expressions up to quadratic order in appropriate order parameters. Using the complete enumeration (given in Appendix A of Ref. 13) of all possible critical points for this model, a stability analysis of the disordered phase is performed in Sec. III. For the special case of parameters considered by CM, their results for the limit of stability are reproduced with minor modifications. In Sec. IV the higher-order terms in the Landau expansion are reanalyzed. For cosine-type ordering we find cubic terms which are missing in the case of sine ordering. The higher-order terms (either cubic or quartic) usually favor triple wave vector ordering. As CM explain this type of ordering is efficient in creating low-energy galleries for the dopants. In Sec. V we construct phase diagrams which show an unexpectedly large variety of ordered phases. In addition to the results of Landau theory we use (a) exact calculations for the thermodynamic potential at zero temperature for periodic structures with small unit cells, (b) an exact relation which relates a phases in which the ith gallery has an occupation probability n_i to one in which n_i is replaced by $1-n_i$, and (c) a numerical analysis of self-consistent field theory for periodic structures with small unit cells. Our results are summarized briefly in Sec. VI.

II. LANDAU EXPANSION: RESULTS TO QUADRATIC ORDER

In this section we review the formulation of mean-field theory. We write the CM Hamiltonian in the form

$$\mathcal{H} = \sum_{\langle ij \rangle} V_{ij}(\theta_i, \theta_j) + \sum_v n_v E_v(\{\theta_{v+\delta}\}) \ , \tag{1}$$

where $\langle ij \rangle$ indicates a sum over pairs of nearest-neighboring sites on a triangular lattice, v is summed over triangular plaquettes, each of which represents a gallery which is either occupied by alkali dopants ($n_v = 1$) or is vacant ($n_v = 0$), and $v+\delta$ labels the three sites at the vertices of plaquette v. In Eq. (1) V_{ij} represents the anisotropic interaction between rotors (i.e., polyacetylene chains),

$$V_{ij} = \alpha \cos(2\theta_i - 2\theta_j) + \beta \cos(2\theta_i - 2\phi_{ij}) \cos(2\theta_j - 2\phi_{ij}), \tag{2}$$

where θ_i is the angle between the plane of the ith polyacetylene molecule (represented by a two-dimensional rotor) and the x axis, ϕ_{ij} is the angle between the vector joining the centers of rotors i and j and the x axis (see Fig. 1), and E_v is the energy of an alkali-metal-filled gallery:

$$E_v = \gamma \sum_\delta \cos(2\theta_{v+\delta} - 2\phi_{v,\delta}) \ , \tag{3}$$

where $\phi_{v,\delta}$ is the angle between the x axis and the vector joining the center of plaquette v and the site labeled $v+\delta$ (see Fig. 2). The local arrangement around an occupied gallery favored by the potential in Eq. (3) is shown in Fig. 3 for both signs of γ. (In this paper we only consider the case $\gamma > 0$.) The interaction E_v competes with the anisotropic potential V_{ij} which favors a herringbone structure for a wide range of values of α and β.[3] In the limit of zero doping the present model is similar to that of Ref. 2 when the crystal potential is such as to force the molecules to line in the plane of the substrate.

The grand potential $\Omega(\mu, T)$ as a function of chemical potential of the dopants, μ, and the temperature, T, is given as the minimum (with respect to variations in the normalized density matrix, ρ) of the trial potential, and is given by

$$\Omega = \min_\rho \Omega_{\rm tr} = \min_\rho \ {\rm Tr}\rho\left[(\mathcal{H} - \mu n) + k_B T \ln \rho\right] \ . \tag{4}$$

Mean-field theory is obtained by assuming a product form for the density matrix:

$$\rho = \prod_i \rho_i(\theta_i) \ \prod_v \rho_v \ , \tag{5}$$

where the density matrix for the rotor at site i is given by

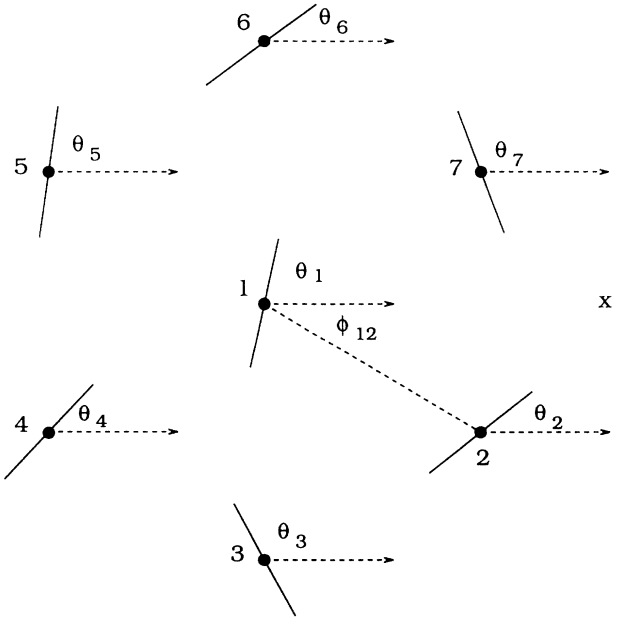

FIG. 1. Definition of angles which specify the anisotropic interactions between rotors.

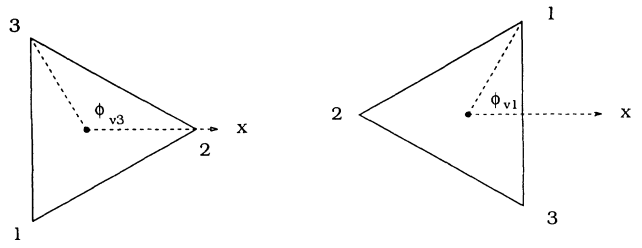

FIG. 2. Left-directed and right-directed plaquettes. The angles $\phi_{v,\delta}$ for the left-directed triangle are 0°, 120°, and 240° for sites 1, 2, and 3, respectively. The "position vector," **R** associated with each triangle is that of site 2.

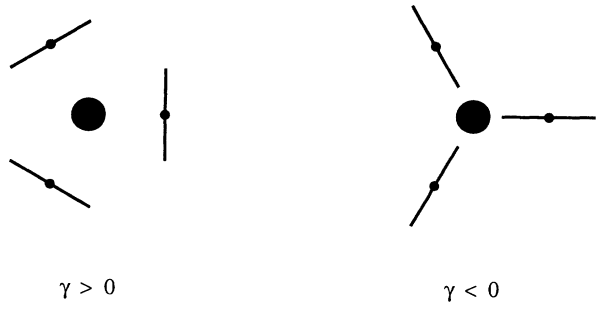

FIG. 3. Minimum energy configuration of rotors surrounding an occupied gallery.

$$\rho_i(\theta_i) = \frac{1}{2\pi}[1 + C_i \cos 2\theta_i + S_i \sin 2\theta_i + C_{i,4} \cos 4\theta_i + S_{i,4} \sin 4\theta_i \cdots] \tag{6}$$

and

$$\rho_v = \frac{1 + (z_v - 1)n_v}{1 + z_v} , \tag{7}$$

where n_v is zero if the gallery v is vacant and is unity if the gallery v is occupied by alkali-metal dopants. Also, in the above "Tr" indicates an integration over all angles θ_i and a sum over all occupation numbers, n_v. Here we introduce the "order parameters," C_i, S_i, $C_{i,4}$, and $S_{i,4}$ which describe the probability distribution for the orientation of molecule i, and z_v which describes the degree of occupation of gallery v. In Eq. (6) we will limit the expansion to terms which affect our results. With this mean-field density matrix the trial potential assumes the form

$$\Omega_{\rm tr} = \sum_{\langle ij \rangle} \langle V_{ij}(\theta_{ij}) \rangle + \sum_i k_B T \langle \ln \rho_i(\theta_i) \rangle + \Omega_v , \tag{8}$$

where we define $\langle A \rangle = \mathrm{Tr}[\prod_i \rho_i(\theta_i) A]$ and Ω_v is the contribution due to the gallery occupation:

$$\Omega_v = \sum_v \left[\langle E_v \rangle - \mu \frac{z_v}{1 + z_v} + k_B T \left(\frac{z_v}{1 + z_v} \ln \frac{z_v}{1 + z_v} + \frac{1}{1 + z_v} \ln \frac{1}{1 + z_v} \right) \right] . \tag{9}$$

Minimizing Ω_v with respect to z_v gives[7]

$$z_v = e^{(\mu - \langle E_v \rangle)/(k_B T)} \tag{10}$$

which leads to

$$\Omega_v = -k_B T \sum_v \ln \left[1 + e^{(\mu - \langle E_v \rangle)/(k_B T)} \right] . \tag{11}$$

Notice that Ω_{tr} depends on $C_{i,4}$ and $S_{i,4}$ only via the entropy term. Keeping only terms which affect the results to fourth order in C_i and S_i we have

$$\langle \ln \rho_i(\theta_i) \rangle = \frac{1}{4}(C_i^2 + S_i^2) + \frac{1}{32}(C_i^2 + S_i^2)^2 + \frac{1}{4}(C_{i,4}^2 + S_{i,4}^2) - \frac{1}{8} C_{i,4}(C_i^2 - S_i^2) - \frac{1}{4} S_{i,4} C_i S_i . \tag{12}$$

Minimizing with respect to $C_{i,4}$ and $S_{i,4}$ yields

$$\langle \ln \rho_i(\theta_i) \rangle = \frac{1}{4}(C_i^2 + S_i^2) + \frac{1}{64}(C_i^2 + S_i^2)^2 . \tag{13}$$

By including the effect of terms involving $\cos 6\theta$ and $\sin 6\theta$ we extended the above calculation to obtain the entropy correct to sixth order in the order parameters. In this way we obtained the mean-field expression for the grand potential in terms of the order parameters C_i and S_i as

$$\Omega_{tr} = \frac{1}{4}\alpha \sum_{\langle ij \rangle} (C_i C_j + S_i S_j) + \frac{1}{4}\beta \sum_{\langle ij \rangle} [C_i C_j \cos^2 2\phi_{ij} + S_i S_j \sin^2 2\phi_{ij} + C_i S_j \sin 2\phi_{ij} \cos 2\phi_{ij} + S_i C_j \sin 2\phi_{ij} \cos 2\phi_{ij}]$$

$$+ k_B T \sum_i \left[\frac{1}{4}(C_i^2 + S_i^2) + \frac{1}{64}(C_i^2 + S_i^2)^2 + \frac{5}{2304}(C_i^2 + S_i^2)^3 \cdots \right] + \sum_{v,p} c_p(\mu) \langle E_v \rangle^p (k_B T)^{1-p} , \tag{14}$$

where c_p is defined so that $\ln\{1+\exp[(\mu/(k_BT)-x]\} = -\sum_p c_p x^p$ and

$$\langle E_v\rangle = \frac{1}{2}\gamma\sum_\delta [C_{v+\delta}\cos 2\phi_{v,\delta} + S_{v+\delta}\sin 2\phi_{v,\delta}] \ . \quad (15)$$

Since $\sum_v\langle E_v\rangle = 0$, we may start the sum over p in Eq. (14) at $p=2$. For instance,

$$c_2(\mu) = -\frac{z}{2(1+z)^2} \ , \quad c_3(\mu) = \frac{z-z^2}{6(1+z)^3} \ ,$$
$$c_4(\mu) = \frac{-z+4z^2-z^3}{24(1+z)^4} \ , \quad (16)$$

where $z=\exp[\mu/(k_BT)]$. In the absence of orientational order $\langle n_v\rangle = z/(1+z)$, in which case $z = \langle n_v\rangle/(1-\langle n_v\rangle)$. For μ negative, $c_3(\mu)$ is positive.

We now introduce Fourier transformed variables via

$$C_i = \sum_{\mathbf{q}} C(\mathbf{q})e^{-i\mathbf{q}\cdot\mathbf{R}_i} \ , \quad (17)$$

$$S_i = \sum_{\mathbf{q}} S(\mathbf{q})e^{-i\mathbf{q}\cdot\mathbf{R}_i} \ . \quad (18)$$

We first express $\langle E_v\rangle$ in terms of these variables, For instance, for "left-directed" triangles, as shown in Fig. 2, we have

$$\langle E_l(\mathbf{R}_l)\rangle = \frac{\gamma}{2}\sum_{\mathbf{q}} e^{-i\mathbf{q}\cdot\mathbf{R}_l}[C(\mathbf{q})\phi_c(\mathbf{q}) + S(\mathbf{q})\phi_s(\mathbf{q})] \quad (19)$$

and similarly for "right-directed" triangles we have

$$\langle E_r(\mathbf{R}_r)\rangle = \frac{\gamma}{2}\sum_{\mathbf{q}} e^{-i\mathbf{q}\cdot\mathbf{R}_r}[C(\mathbf{q})\phi_c(\mathbf{q})^* + S(\mathbf{q})\phi_s(\mathbf{q})^*] \ , \quad (20)$$

where $\mathbf{R}_r$ and $\mathbf{R}_l$ are the locations of the vertices specified in Fig. 2 for the plaquette in question and

$$\phi_c(\mathbf{q}) = 1 - c_y(\mathbf{q})e^{-i\sqrt{3}q_x/2} \ , \quad (21)$$

$$\phi_s(\mathbf{q}) = -i\sqrt{3}s_y(\mathbf{q})e^{-i\sqrt{3}q_x/2} \ , \quad (22)$$

where

$$c_y(\mathbf{q}) = \cos(q_y/2), \quad s_y(\mathbf{q}) = \sin(q_y/2) \ . \quad (23)$$

Then the quadratic part of Ω_{tr} is

$$N^{-1}\Omega^{(2)} = \frac{1}{2}\sum_{\mathbf{q}} [C(-\mathbf{q}),\ S(-\mathbf{q})]\,\Lambda(\mathbf{q})\begin{bmatrix} C(\mathbf{q}) \\ S(\mathbf{q})\end{bmatrix} \ , \quad (24)$$

where

$$\Lambda_{cc}(\mathbf{q}) = \frac{1}{2}k_BT + \frac{1}{4}\alpha\gamma(\mathbf{q}) + \frac{1}{4}\beta\gamma_{cc}(\mathbf{q}) - 2x|\phi_c(\mathbf{q})|^2 \ , \quad (25)$$

$$\Lambda_{ss}(\mathbf{q}) = \frac{1}{2}k_BT + \frac{1}{4}\alpha\gamma(\mathbf{q}) + \frac{1}{4}\beta\gamma_{ss}(\mathbf{q}) - 2x|\phi_s(\mathbf{q})|^2 \ , \quad (26)$$

$$\Lambda_{sc}(\mathbf{q}) = \Lambda_{cs}(\mathbf{q}) = \frac{1}{4}\beta\gamma_{sc}(\mathbf{q}) - 2x\mathrm{Re}\,\{\phi_c(\mathbf{q})\phi_s(-\mathbf{q})\} \ , \quad (27)$$

where

$$x = \gamma^2 z/[4k_BT(1+z)^2] \quad (28)$$

and

$$\gamma(\mathbf{q}) = 4c_y(\mathbf{q})^2 - 2 + 4c_x(\mathbf{q})c_y(\mathbf{q}) \ , \quad (29)$$

$$\gamma_{cc}(\mathbf{q}) = 4c_y(\mathbf{q})^2 - 2 + c_x(\mathbf{q})c_y(\mathbf{q}) \ , \quad (30)$$

$$\gamma_{ss}(\mathbf{q}) = 3c_y(\mathbf{q})c_x(\mathbf{q}) \ , \quad (31)$$

$$\gamma_{sc}(\mathbf{q}) = -\sqrt{3}s_x(\mathbf{q})s_y(\mathbf{q}) \ , \quad (32)$$

where

$$c_x(\mathbf{q}) = \cos(\sqrt{3}q_x/2) \ , \quad s_x(\mathbf{q}) = \sin(\sqrt{3}q_x/2) \ . \quad (33)$$

The above results differ slightly from those of CM. In their Eq. (7a), 3/2 is a misprint (not affecting their results) and should be replaced by 1/2. Likewise γ_2 should be identified with $\cos(q_y a/2)$ to reproduce the results for the undoped system,[3] providing the free energy is normalized in the same way in both references. More serious, however, is that where we have $2x$ in Eqs. (25), (26), and (27), their results correspond to having $4x$. As a result of this, our results indicate that their phase boundary for the disordered phase in their Fig. 2 corresponds to $\alpha=-1$, $\beta=2$, and $\gamma=3\sqrt{2}$, rather than $\gamma=3$, as we find here.

III. LANDAU EXPANSION: STABILITY ANALYSIS

At a μ-dependent temperature, $T_0(\mu)$, the disordered phase becomes locally unstable. This temperature is determined as the highest temperature at which one of the eigenvalues of the Λ matrix becomes zero. The wave vector $\mathbf{q}_0$ for which this happens selects the star of wave vector(s) needed to form the ordered phase. In Appendix A of Ref. 13 we locate all wave vectors at which extrema can conceivably appear for the present model. We find that $\mathbf{q}_0$ must lie in a high-symmetry direction. Here we use that information to carry out an analysis which, for simplicity, is confined to a restricted region in parameter space. To treat negative α we arbitrarily set $\alpha=-1$, and we consider only positive β. Thereby we include the parameter values considered by CM: $\alpha=-1$ and $\beta=2$. A simple way to find the instability temperature, the wave vector associated with this instability, and the associated eigenvector, is to compare the eigenvalues of

the fluctuation matrix at the critical points listed in Appendix A of Ref. 13. We did this numerically for $\alpha = -1$ over the region $0.5 < \beta < 9.5$ and the results are given in Fig. 4. There we show what kind of instability occurs in the fluctuation matrix as a function of parameters. The instability temperature as a function of β and x is not indicated in this diagram. Also, if the transition is a discontinuous one, that is not indicated either, but will be discussed later in Sec. V. For $\beta = 2$ the results in Fig. 4 reproduce those of CM (apart from replacing γ by $\gamma\sqrt{2}$). However, as we shall see, even within mean-field theory, the phase diagram is quite a rich one and differs from what one would predict on the basis of Fig. 4 due to the occurrence of first-order phase transitions.

We now discuss the results shown in Fig. 4. In describing our results it is useful to note that the fluctuation matrix is diagonal if either s_x or s_y vanishes. Except when the instability occurs at zero wave vector, we will classify ordering by the type of instability that occurs for $q_x = 2\pi/\sqrt{3}$. For small β ($\beta < 4/3$) and small x, the scalar interaction (proportional to α) dominates and the instability is towards a "ferromagnetic" (F) phase in which all rotors are parallel to one another. In this phase, since the cosine and sine eigenvalues are degenerate at zero wave vector, one has an x-y-like phase. Presumably, the lattice will provide a sixfold anisotropy. The mean-field transition temperature is given by

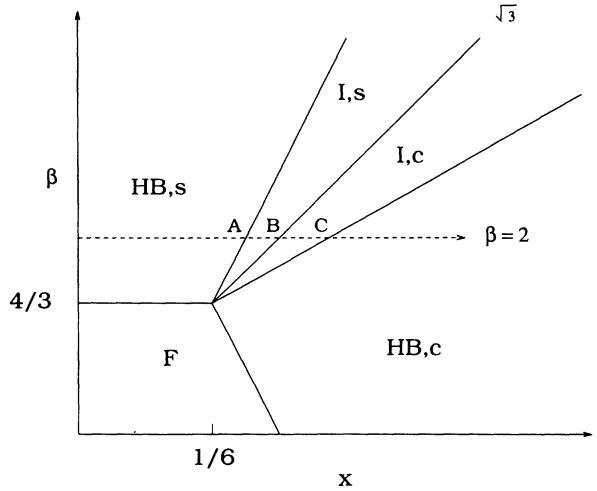

FIG. 4. Instability diagram for the diluted anisotropic rotor model for $\alpha = -1$. The regions shown indicate the instability *in the quadratic term* of the Landau expansion. In most of the HB,s region the ordering transition which occurs as the temperature is lowered is a continuous transition (at least within mean-field theory) from the disordered phase to the HB,s phase. Similarly, within the F region, the ordering transition is an x-y-like transition. For most other values of the parameters the quadratic instability is probably preempted by first-order transitions. For examples of this, see Sec. V. There we discuss the phase diagram for $\alpha = -1$ and $\beta = 2$ in the T-μ plane, which corresponds to the dashed line $\beta = 2$. Also I, s (I, c) denotes incommensurate sine (cosine) ordering and HB,c denotes herringbone cosine ordering. The line labeled $\sqrt{3}$ corresponds to $\sqrt{3}$ ordering.

$$k_B T_{xy} = 3 - \frac{3}{2}\beta \ . \tag{34}$$

As x is increased, the dominant instability shifts to a herringbone phase. For $\beta < 4/3$, this crossover occurs at

$$x_{F\to \mathrm{HB},c} = (4-\beta)/16 \ . \tag{35}$$

For $\mathbf{q} = \mathbf{Q}_A$, as defined in Fig. 5, the instability is in Ω_{cc}, so we call this a herringbone cosine (HB,c) phase (which is illustrated in Fig. 6) and the instability temperature is given by

$$k_B T_{\mathrm{HB},c} = 16x - 1 - \frac{1}{2}\beta \ . \tag{36}$$

Simultaneous instabilities occur also at the other equivalent herringbone wave vectors $\mathbf{Q}_B$ and $\mathbf{Q}_C$, shown in Fig. 5.

For $\beta > 4/3$ and small x the instability is to a herringbone phase. For $\mathbf{q} = \mathbf{Q}_A$ the instability is in Ω_{ss}, so we call this a herringbone sine (HB,s) phase (see Fig. 6). Its instability temperature is given by

$$k_B T_{\mathrm{HB},s} = \frac{3}{2}\beta - 1 \ . \tag{37}$$

As x is increased beyond a critical value,

$$x_{\mathrm{HB},s\to I,s} = \frac{3\beta+4}{48} \ , \tag{38}$$

the dominant instability is to an incommensurate phase. In this phase one of the unstable wave vectors, $\boldsymbol{\tau}_1$, is given by

$$\boldsymbol{\tau}_1 = \mathbf{Q}_A + 2\cos^{-1}\left(\frac{3\beta-4}{8(6x-1)}\right)\hat{\mathbf{j}} \ . \tag{39}$$

For this wave vector the instability occurs in Λ_{ss}, and we call this phase an incommensurate sine (I, s) phase. In this phase the star of the unstable wave vector again consists of the six wave vectors, $\boldsymbol{\tau}_i$ for $i = 1, 6$, shown in

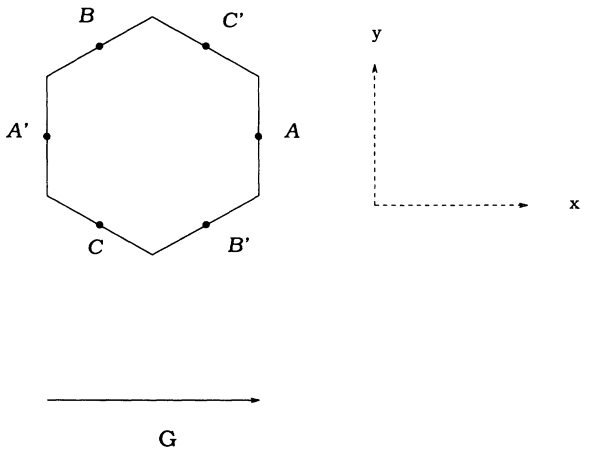

FIG. 5. Location of the herringbone vectors, $\mathbf{Q}_A$, $\mathbf{Q}_B$, and $\mathbf{Q}_C$ one the edge of the Brillouin zone. The magnitude of each vector is $4\pi/(3a)$ where $a = 1$ is the lattice constant. A (big) reciprocal lattice vector is shown.

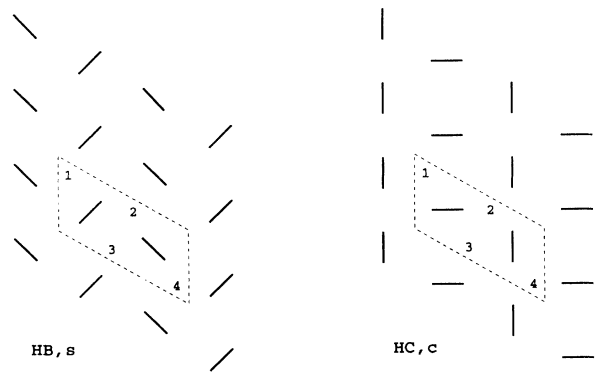

FIG. 6. The ordered phases in which a single herringbone wave vector has condensed with a unit cell (indicated by dashed lines) containing two rotors and four galleries. (a) Left: the HB sine phase in which each sublattice of rotors makes a 45° angle with the HB wave vector. Referred to that direction $\langle \sin(2\theta_i)\rangle = \pm\sigma$, where σ measures the degree of ordering. In the HB,s phase all galleries are equally populated. (b) Right: the HB cosine phase in which each sublattice of rotors makes either a 0° or 90° angle with the HB wave vector. Referred to that direction $\langle \cos(2\theta_i)\rangle = \pm\sigma$, where σ measures the degree of ordering. In the HB,c phase galleries 1 and 3 are equivalent and are preferentially occupied compared to galleries 2 and 4 (which are also equivalent to one another.)

Fig. 7. The instability temperature is given by

$$k_B T_{I,s} = 12x - 1 + \frac{(3\beta - 4)^2}{32(6x - 1)} \ . \tag{40}$$

As x is increased still further the instability shifts to the cosine channel. The critical value of x for this shift is given by

$$x_{I,s \to I,c} = \beta/8 \ . \tag{41}$$

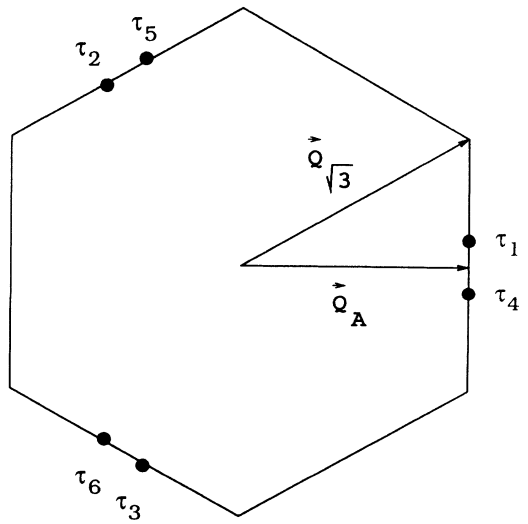

FIG. 7. Location and labeling of the incommensurate vectors which become unstable for the present model. The herringbone and $\sqrt{3}$ wave vectors are $\mathbf{Q}_A$ and $\mathbf{Q}_{\sqrt{3}}$, respectively.

At this critical value of x, $\boldsymbol{\tau}_1$ is equal to a $\sqrt{3}$ wave vector. The wave vector, $\boldsymbol{\tau}_1$, in the incommensurate cosine (I,c) phase is given by

$$\boldsymbol{\tau}_1 = \mathbf{Q}_A + 2\cos^{-1}\left(\frac{16x + \beta - 4}{8(\beta - 1 - 2x)}\right)\hat{\mathbf{j}} \ . \tag{42}$$

For this wave vector the instability occurs in Λ_{cc}. In this phase the star of the unstable wave vector consists of six wave vectors, as shown in Fig. 7. The instability temperature is given by

$$k_B T_{I,c} = 4x + \beta - 1 + \frac{(16x + \beta - 4)^2}{32(\beta - 1 - 2x)} \ . \tag{43}$$

Finally, for x larger than

$$x_{I,c \to \mathrm{HB},c} = (7\beta - 4)/32 \tag{44}$$

the instability is again into a herringbone phase, but now a herringbone cosine (HB,c) phase. Here, for $\mathbf{q} = \mathbf{Q}_A$, the instability is in Λ_{cc} and occurs at the instability temperature

$$k_B T_{\mathrm{HB},c} = 16x - 1 - \frac{1}{2}\beta \ . \tag{45}$$

Consider the multicritical point at $\beta = 4/3$ and $x = 1/6$, at which all the phases are simultaneously unstable. (This multicritical point could be modified if some of the transitions are discontinuous.) For these values of parameters, Λ is diagonal *with* $\mathbf{q}$*-independent degenerate* diagonal elements, $\Lambda_{ii} = \frac{1}{2}(k_B T - 1)$. As in the *kagomé* case,[14] the degeneracy is removed by thermal fluctuations.[15,16]

For completeness we display the form of the free energy to quadratic order in the critical order parameters. In so doing, it is useful to transform to "normal modes." For instance, when the instability occurs at the herringbone vectors, we write

$$S(\mathbf{Q}_A) = \sqrt{2}X_1 \ , \tag{46}$$

$$C(\mathbf{Q}_A) = \sqrt{2}Y_1 \ , \tag{47}$$

$$S(\mathbf{Q}_B) = -\frac{1}{\sqrt{2}}X_2 - \frac{\sqrt{3}}{\sqrt{2}}Y_2 \ , \tag{48}$$

$$C(\mathbf{Q}_B) = \frac{\sqrt{3}}{\sqrt{2}}X_2 - \frac{1}{\sqrt{2}}Y_2 \ , \tag{49}$$

$$S(\mathbf{Q}_C) = -\frac{1}{\sqrt{2}}X_3 + \frac{\sqrt{3}}{\sqrt{2}}Y_3 \ , \tag{50}$$

$$C(\mathbf{Q}_C) = -\frac{\sqrt{3}}{\sqrt{2}}X_3 - \frac{1}{\sqrt{2}}Y_3 \ . \tag{51}$$

In terms of these variables the free energy is diagonal:

$$N^{-1}\Omega^{(2)} = \frac{1}{2}[T - T_s(\mu)][X_1^2 + X_2^2 + X_3^2] + \frac{1}{2}[T - T_c(\mu)][Y_1^2 + Y_2^2 + Y_3^2] , \quad (52)$$

where $T_s(\mu)$ $[T_c(\mu)]$ is the instability temperature for sine (cosine) fluctuations at wave vector $\mathbf{Q}_A$.

In the incommensurate phases, the above is modified by introduction of a phase for each variable. Relative to the herringbone phase, each wave vector bifurcates, as illustrated in Fig. 7, to produce the incommensurate phase. Then, for instance, we set

$$S(\tau_1) = X_1 , \quad S(\tau_4) \equiv S(-\tau_1) = X_4 = X_1^* , \quad (53)$$

$$C(\tau_1) = Y_1 , \quad C(\tau_4) \equiv C(-\tau_1) = Y_4 = Y_1^* , \quad (54)$$

and similarly for the other wave vectors. (We introduced the factors $\sqrt{2}$ in the normalization of the herringbone modes so that the quadratic free energy would be the same for commensurate and incommensurate cases.) Then Eq. (52) continues to hold, except that the order parameters are complex, X_i^2 is replaced by $|X_i|^2$, and Y_i^2 is replaced by $|Y_i|^2$. In any case, the dominant instability is the one with the higher instability temperature.

IV. LANDAU EXPANSION: RESULTS TO HIGHER ORDER

In this section we analyze higher-order terms in the Landau expansion. If there are cubic terms in the Landau expansion, the transition will be discontinuous. Also, the nature of the higher-order terms will dictate whether condensation takes place at a single wave vector or simultaneously at all wave vectors equivalent by symmetry. In addition, higher-order terms can fix the relative phases with which the order parameters condense. Such terms describe phase locking or devil's staircase behavior, as found, for instance, in the Frankel-Kontorova model[17] and in similar spin models.[18,12,19]

Higher than quadratic terms in the Landau expansion come from two sources in Eq. (14): the entropy term and the term involving $\langle E_v \rangle$. Clearly cubic terms can only come from the latter source. We first analyze possible cubic terms. For powers of $\langle E_v \rangle$ we use

$$\begin{aligned}\langle E_l(\mathbf{R})\rangle = \frac{1}{2}\gamma\{&e^{-i\tau_1\cdot\mathbf{R}}[i\sqrt{3}s_y X_1 + (1+c_y)Y_1] + e^{i\tau_1\cdot\mathbf{R}}[-i\sqrt{3}s_y X_4 + (1+c_y)Y_4] \\ &+e^{-i\tau_2\cdot\mathbf{R}}[-i\sqrt{3}s_y X_2 - (1+c_y)Y_2]e^{ik/2} + e^{i\tau_2\cdot\mathbf{R}}[i\sqrt{3}s_y X_5 - (1+c_y)Y_5]e^{-ik/2} \\ &+e^{-i\tau_3\cdot\mathbf{R}}[-i\sqrt{3}s_y X_3 - (1+c_y)Y_3]e^{-ik/2} + e^{i\tau_3\cdot\mathbf{R}}[i\sqrt{3}s_y X_6 - (1+c_y)Y_6]e^{ik/2}\} , \end{aligned} \quad (55)$$

where $\tau_{1,y} = k$ specifies the incommensurate part of the wave vectors and $s_y = \sin(k/2)$ and $c_y = \cos(k/2)$. In the above we noted that $-\tau_i$ and τ_{i+3} are equivalent. For herringbone wave vectors, set $k = 0$, replace γ by $\gamma\sqrt{2}$, and omit the terms involving X_i and Y_i for $i > 3$. In writing these expressions we only keep contributions from fluctuations which are potentially critical. Note that since $\phi_s(0) = \phi_c(0)$, $\langle E_l(\mathbf{R})\rangle$ has no contributions involving zero wave vector. Also, in the commensurate (herringbone) phase $s_y = 0$ and the critical sine modes do not couple to the vacancy free energy. To obtain the analogous expression for $\langle E_r(\mathbf{R})\rangle$ replace s_y by $-s_y$ and $e^{ik/2}$ by $e^{-ik/2}$.

A. Sine phases

We start by analyzing the higher-order terms in the Landau expansion for the sine phases. To treat these phases, we focus on the X variables, which are the critical variables for sine ordering. For the cubic terms we have

$$N^{-1}\delta\Omega^{(3)} = \frac{c_3(\mu)}{N(k_BT)^2}\sum_{\mathbf{R}}\left(\langle E_l(\mathbf{R})\rangle^3 + \langle E_r(\mathbf{R})\rangle^3\right) . \quad (56)$$

We see that

$$N^{-1}\sum_{\mathbf{R}}\langle E_l(\mathbf{R})\rangle^3 = 6\left(\frac{i\sqrt{3}\gamma s_y}{2}\right)^3 \times (X_1X_2X_3 - X_4X_5X_6) . \quad (57)$$

Since this result is an odd function of s_y, we see that $\delta\Omega^{(3)}$, as given by Eq. (56), vanishes in this case. Furthermore, the entropic terms are all even order. Therefore sine phases, whether commensurate or incommensurate, do not allow any cubic terms.

We now consider the quartic terms arising from the entropy. For the commensurate (HB) case we write[2]

$$S_i^2 + C_i^2 = 2[X_1^2 + X_2^2 + X_3^2 - X_1X_2e^{i\mathbf{Q}_C\cdot\mathbf{R}} - X_2X_3e^{i\mathbf{Q}_A\cdot\mathbf{R}} - X_3X_1e^{i\mathbf{Q}_B\cdot\mathbf{R}}] . \quad (58)$$

Thus the fourth-order contribution to the free energy is

$$\begin{aligned}N^{-1}\delta\Omega^{(4)} &= \frac{k_BT}{64N}\sum_i\left(S_i^2 + C_i^2\right)^2 \\ &= \frac{k_BT}{16}\{[X_1^2 + X_2^2 + X_3^2]^2 + X_1^2X_2^2 + X_2^2X_3^2 + X_3^2X_1^2\} . \end{aligned} \quad (59)$$

Note that the anisotropy favors the condensation of a *single* wave vector in preference to simultaneous condensation of *all* wave vectors in the star. In view of the fact that the present model is similar to that used in Ref. 2

in the limit when their V_c is large and negative (forcing the molecules to lie in the plane), this result is expected.

The situation changes when the wave vector becomes incommensurate. As we have seen, there are still no cubic terms. Next consider the fourth-order entropic contributions. In terms of the critical amplitudes of the six incommensurate wave vectors, we have

$$S_i = e^{-i\tau_1\cdot\mathbf{R}_i}X_1 + e^{i\tau_1\cdot\mathbf{R}_i}X_1^* - \frac{1}{2}e^{-i\tau_2\cdot\mathbf{R}_i}X_2 - \frac{1}{2}e^{i\tau_2\cdot\mathbf{R}_i}X_2^* - \frac{1}{2}e^{-i\tau_3\cdot\mathbf{R}_i}X_3 - \frac{1}{2}e^{i\tau_3\cdot\mathbf{R}_i}X_3^* , \quad (60)$$

$$C_i = \frac{\sqrt{3}}{2}[e^{-i\tau_2\cdot\mathbf{R}_i}X_2 + e^{i\tau_2\cdot\mathbf{R}_i}X_2^* - e^{-i\tau_3\cdot\mathbf{R}_i}X_3 - e^{i\tau_3\cdot\mathbf{R}_i}X_3^*] . \quad (61)$$

When we sum a fourth-order contribution over i, a nonzero result only occurs when the sum of four incommensurate wave vectors is zero modulo the reciprocal lattice. We find

$$N^{-1}\delta\Omega^{(4)} = \frac{k_BT}{64N}\sum_i \left(S_i^2 + C_i^2\right)^2 \sim \frac{3k_BT}{32}\left[|X_1|^2 + |X_2|^2 + |X_3|^2\right]^2 . \quad (62)$$

The important result here is that so far we have not obtained any anisotropy at all. So far, then, there is no discrimination between single and triple wave vector states.

It is interesting to observe the difference between the results in Eqs. (59) and (62). The discontinuity is an example of phase locking and can be represented by a term

$$N^{-1}\delta\Omega_{\rm lock} \equiv N^{-1}\delta\Omega_{\rm HB}^{(4)} - N^{-1}\delta\Omega^{(4)}(\mathbf{q}\neq\mathbf{Q}_A) = -\frac{k_BT}{32}\delta_{\mathbf{q},\rm HB}(X_1^4 + X_2^4 + X_3^4) , \quad (63)$$

where $\delta_{\mathbf{q},\rm HB}$ is unity if the wave vector $\mathbf{q}$ of the structure is a herringbone vector, and is zero otherwise. This result shows that phase locking (into the HB state) is accompanied by an anisotropy which favors the single wave vector phase.

For the incommensurate sine phase there are additional fourth-order terms coming from Ω_v. We will express these contributions in terms of the incommensurate part, k, of the wave vector, where (see Fig. 7)

$$\tau_1 = \mathbf{Q}_A + k\hat{\mathbf{j}} \quad (64)$$

and similarly for the other τ_i. Note that k ranges from 0 (for the HB wave vector) to $2\pi/3$ (for the $\sqrt{3}$ wave vector). There are two fourth-order contributions, the first obtained by expanding Ω_v to fourth order in the critical amplitudes X_i. The second is an induced term obtained by the effect of a third-order term in Ω_v which involves two critical amplitudes and one noncritical amplitude. Minimization with respect to the noncritical amplitude then gives induced terms which are fourth order in the critical amplitudes.[2] As we shall see, these contributions are analytic in k in contrast to that written in Eq. (63).

The first type of term is

$$N^{-1}\delta_1\Omega^{(4)} = \frac{c_4}{N(k_BT)^3}\sum_{\mathbf{R}}\left(\langle E_l(\mathbf{R})\rangle^4 + \langle E_r(\mathbf{R})\rangle^4\right) = \frac{2c_4}{N(k_BT)^3}\sum_{\mathbf{R}}\langle E_l(\mathbf{R})\rangle^4 . \quad (65)$$

Using Eq. (55) we find that

$$N^{-1}\delta_1\Omega^{(4)} = \lambda_0[|X_1|^4 + |X_2|^4 + |X_3|^4 + 4(|X_1|^2|X_2|^2 + |X_2|^2|X_3|^2 + |X_3|^2|X_1|^2)] , \quad (66)$$

where

$$\lambda_0 = \frac{27}{4}c_4k_BT\left(\frac{\gamma\sin(k/2)}{k_BT}\right)^4 . \quad (67)$$

To obtain the induced contribution we start from

$$\frac{\delta\Omega^{(3)}}{N} = -\frac{9c_3\gamma^3\sin^2(k/2)}{8N(k_BT)^2}\sum_{\mathbf{R}}\Bigg\{[e^{-i\tau_1\cdot\mathbf{R}}X_1 - e^{i\tau_1\cdot\mathbf{R}}X_4 - e^{-i\tau_2\cdot\mathbf{R}}X_2e^{ik/2} + e^{i\tau_2\cdot\mathbf{R}}X_5e^{-ik/2} - e^{-i\tau_3\cdot\mathbf{R}}X_3e^{-ik/2} + e^{i\tau_3\cdot\mathbf{R}}X_6e^{ik/2}]^2\sum_{\mathbf{q}}e^{-i\mathbf{q}\cdot\mathbf{R}}[C(\mathbf{q})\phi_c(\mathbf{q}) + S(\mathbf{q})\phi_s(\mathbf{q})]\Bigg\}$$
$$-\frac{9c_3\gamma^3\sin^2(k/2)}{8N(k_BT)^2}\sum_{\mathbf{R}}\Bigg\{[e^{-i\tau_1\cdot\mathbf{R}}X_1 - e^{i\tau_1\cdot\mathbf{R}}X_4 - e^{-i\tau_2\cdot\mathbf{R}}X_2e^{-ik/2} + e^{i\tau_2\cdot\mathbf{R}}X_5e^{ik/2} - e^{-i\tau_3\cdot\mathbf{R}}X_3e^{ik/2} + e^{i\tau_3\cdot\mathbf{R}}X_6e^{-ik/2}]^2\sum_{\mathbf{q}}e^{-i\mathbf{q}\cdot\mathbf{R}}[C(\mathbf{q})\phi_c(\mathbf{q})^* + S(\mathbf{q})\phi_s(\mathbf{q})^*]\Bigg\} . \quad (68)$$

We must minimize the term written in Eq. (68) with the quadratic terms (taking both signs of wave vectors) written in Eq. (24). So doing yields an induced quartic interaction of the form

$$\delta_2\Omega^{(4)} = \lambda_1\left(|X_1|^4 + |X_2|^4 + |X_3|^4\right) + \lambda_2\left(|X_1|^2|X_2|^2 + |X_2|^2|X_3|^2 + |X_3|^2|X_1|^2\right) . \quad (69)$$

In Appendix B of Ref. 13 we evaluate these coefficients as

$$\lambda_1 = -\frac{81c_3^2\gamma^6\sin^8(k/2)}{4(k_BT)^4\Lambda_{cc}(2k\hat{\mathbf{j}})} . \tag{70}$$

$$\lambda_2 = -\frac{81c_3^2\gamma^6\sin^4(k/2)}{4(k_BT)^4}\left[\frac{[\cos k+\cos(k/2)]^2}{\Lambda_{cc}[(2\pi/\sqrt{3})\hat{\mathbf{i}}+\sqrt{3}k\hat{\mathbf{i}}]} + \frac{[1+\cos(k/2)]^2}{\Lambda_{cc}(\boldsymbol{\tau}_1)}\right] . \tag{71}$$

Thus, the sum of the fourth-order contributions is

$$\delta\Omega^{(4)} = u_s\left(|X_1|^2+|X_2|^2+|X_3|^2\right)^2 + v_s\left(|X_1|^2|X_2|^2+|X_2|^2|X_3|^2+|X_3|^2|X_1|^2\right) , \tag{72}$$

where

$$u_s = \frac{3}{32}k_BT+\lambda_0+\lambda_1 \tag{73}$$

and

$$v_s = 2\lambda_0-2\lambda_1+\lambda_2 . \tag{74}$$

Two important aspects of this result are (a) the sign of v_s and the sign of the overall fourth-order term in the easy direction: $u_4 \equiv \mathrm{Min}\{u_s, u_s+(v_s/3)\}$. The sign of v_4 will indicate whether or not the transition is continuous (assuming this transition is not preempted by another first-order transition). Assuming a continuous transition, or at least a sufficiently weak first-order transition, we can say that if v_s is positive, we have a single wave vector, i.e., what CM call a striped phase. Otherwise we have what CM call a hexagonally modulated phase. In Fig. 8 we show u_s and v_s as functions of μ, evaluated at the instability temperature $T_0(\mu)$ for $\alpha=-1$, $\beta=2$, and $\gamma=3$. One sees that u_s is positive, i.e., this transition is continuous (assuming no other transition intervenes) only rather close to the point A in Fig. 4 (where the herringbone phase appears). Since v_s is always negative (except very close to $\mu=0$), the triple wave vector incommensurate state is favored over the striped incommensurate phase. (This is reasonable, inasmuch as it is the former phase which tends to make favorable galleries for the dopants.) At point B in Fig. 4, the cubic term begins to become nonzero, as we shall see in a moment. We will discuss this multicritical point further in the next section, when we describe numerically obtained phase diagrams.

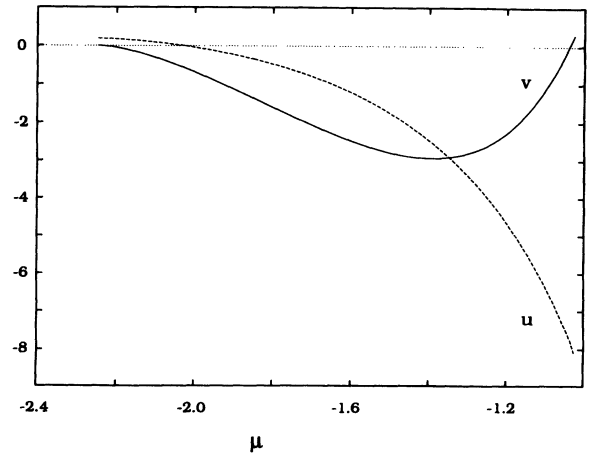

FIG. 8. Landau parameters u_s v_s of Eq. (74) versus μ for the incommensurate sine (I,s) phase, for $\alpha=-1$ and $\beta=2$, and $\gamma=3$. Point A in Fig. 4 corresponds to $\mu=-2.246$ and point B to $\mu=0$.

For the incommensurate phase we have not yet said anything about how the phases associated with the three wave vectors are fixed, if at all. In general, two of these phases will be associated with the origin of the structure and if these two phases are completely free, one will have a two-dimensional phason. It seems likely that there are regimes of such behavior, as in the Frankel-Kontorova model.[17] The sum of the three phases will be fixed by a sixth-order term. Note that the quartic terms dictate that the amplitudes of all the normal modes should be equal when they order. So we write

$$X_1 = X_4^* = Ze^{i\phi_1} , \quad X_2 = X_5^* = Ze^{i\phi_2} , \quad X_3 = X_6^* = Ze^{i\phi_3} , \tag{75}$$

where Z is positive real. Then there will be a sixth-order term proportional to

$$K_6\left(X_1^2X_2^2X_3^2+X_4^2X_5^2X_6^2\right) = 2K_6Z^6\cos(2\phi_1+2\phi_2+2\phi_3) , \tag{76}$$

which will fix the sum of the phases to either be 0 or to be $\pi/2$, depending on the sign of the constant, K_6. Since the calculation of K_6 is rather tedious, we omit it.

B. Cosine phases

In this section we consider the form of the higher-order terms in the cosine phases. We start with the cubic terms. For this purpose we rewrite Eq. (55) keeping only the cosine (Y) variables. Thus, for the incommensurate cosine phase we write

$$\langle E_l(\mathbf{R})\rangle = \frac{1}{2}\gamma(1+c_y)(e^{-i\boldsymbol{\tau}_1\cdot\mathbf{R}}Y_1 - e^{-i\boldsymbol{\tau}_2\cdot\mathbf{R}}Y_2 - e^{-i\boldsymbol{\tau}_3\cdot\mathbf{R}}Y_3 + e^{-i\boldsymbol{\tau}_4\cdot\mathbf{R}}Y_4 - e^{-i\boldsymbol{\tau}_5\cdot\mathbf{R}}Y_5 - e^{-i\boldsymbol{\tau}_6\cdot\mathbf{R}}Y_6) \tag{77}$$

so that for the I,c phase the result is

$$\delta\Omega_{I,c}^{(3)} = \frac{c_3}{(k_BT)^2}\sum_{\mathbf{R}}\left(\langle E_l(\mathbf{R})\rangle^3+\langle E_r(\mathbf{R})\rangle^3\right) = \frac{3Nc_3\gamma^3}{2(k_BT)^2}(1+c_y)^3\left(Y_1Y_2Y_3+Y_4Y_5Y_6\right) . \tag{78}$$

Writing $Y_i = Z_ie^{i\phi_i}$ for $i=1,2,3$, this gives

$$\delta\Omega^{(3)}_{I,c} = NK_3 Z_1 Z_2 Z_3 \cos(\phi_1 + \phi_2 + \phi_3) \ , \tag{79}$$

where

$$K_3 = \frac{3c_3\gamma^3}{(k_BT)^2}(1 + c_y)^3 \ . \tag{80}$$

For the commensurate HB,c phase, we drop the term $Y_4Y_5Y_6$ in Eq. (78) and replace Y_i by $\sqrt{2}Y_i$ to get

$$\delta\Omega^{(3)}_{\mathrm{HB},c} = (81\sqrt{2}/8)Nc_3\gamma^3(k_BT)^{-2}Y_1Y_2Y_3 \ , \tag{81}$$

where the Y's are real.

For the I,c phase, $\delta\Omega^{(3)}$ is minimized by taking $Z_i = Z$ and appropriately choosing the sum of the phases. As in the case of the sine phases, we expect that for the I,c phase there will be regimes in which the two other phases are free phason variables. To see the meaning of fixing the sum phases in Eq. (79), it is simplest to consider the commensurate HB,c phase. Here the Y's are real and we set $Y_i = \sigma_i Z$, where Z is real positive, each σ_i is either $+1$ or -1 and the cubic term forces all the amplitudes to be equal to one another. The construction of the resulting triple wave vector states, having four rotors per unit cell, is similar to that done in Ref. 2. First observe from Eqs. (6) and (46)–(51) that the density matrix is

$$2\pi\rho_{\mathbf{R}}(\theta_i) - 1 = \sqrt{2}Z\left[\left(\sigma_A e^{i\mathbf{Q}_A\cdot\mathbf{R}} - \frac{1}{2}\sigma_B e^{i\mathbf{Q}_B\cdot\mathbf{R}} - \frac{1}{2}\sigma_C e^{i\mathbf{Q}_C\cdot\mathbf{R}}\right)\cos(2\theta_{\mathbf{R}}) + \frac{\sqrt{3}}{2}\left(\sigma_C e^{i\mathbf{Q}_C\cdot\mathbf{R}} - \sigma_B e^{i\mathbf{Q}_B\cdot\mathbf{R}}\right)\sin(2\theta_{\mathbf{R}})\right] \ . \tag{82}$$

Suppose $c_3\gamma > 0$. (Since we assume that $\gamma > 0$, this condition implies that $\mu < 0$.) If one chooses all the σ's to be negative, one minimizes the cubic term in the free energy [see Eq. (81)], whereas taking all the σ's to be positive would minimize the free energy for the opposite sign of $c_3\gamma$. The four states obtained by choosing the σ's so that their product is positive (or negative) differ from one another by different origins for the unit cell. The state with all σ's negative is shown in Fig. 9(a) and that with all the σ's positive is shown in Fig. 9(b). As in the triple wave vector sine state, called a pinwheel state,[2] one rotor is disordered and the other three each assume a different orientation. (It is not expected that this phase, with complete disorder in one sublattice, could remain the true equilibrium state down to zero temperature.) The gallery occupation energies for these two triple wave vector cosine states are given in Table I. Again, the four choices of σ's correspond to the four choices of origin of the disordered rotor in the unit cell. (A similar analysis shows that for the triple wave vector, or pinwheel sine phase, shown in Fig. 10, all eight choices of the σ's lead to states which are equivalent by symmetry and in fact all the gallery occupation energies in the pinwheel

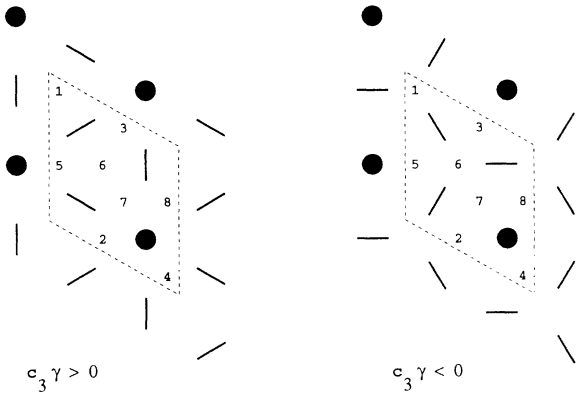

FIG. 9. The two herringbone or pinwheel cosine (PWc) triple wave vector states. The filled circles represent orientationally disordered rotors. In each case the unit cell containing four rotors and eight galleries is shown by dashed lines. In each case one see that galleries 1 and 6 are equivalent and the other galleries are all mutually equivalent. (a) Left: the state corresponding to the choice of the three phase factors, σ_i, such that their product is negative. The eight galleries in the unit cell are numbered and have occupation energies listed in Table I. (b) Right: the state corresponding to the product of the σ_i being positive. Changing the sign of σ_i induces a change in the orientation of the ith rotor by 90°. Note the most negative occupation energy for galleries 1 and 6 in the left-hand structure and the most positive occupation energy for these galleries in the right-hand structure. Thus when the galleries are less (more) than half filled, the left-hand (right-hand) structure is favored.

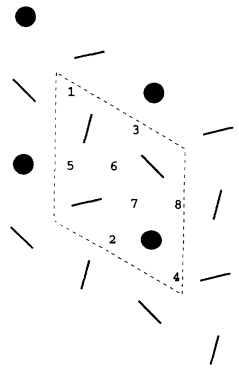

FIG. 10. As in Fig. 9, but for the triple wave vector [pinwheel (Ref. 2)] sine phase. In contrast to the galleries in Fig. 9, all galleries here have zero occupation energy. Also there are eight equivalent such pinwheel states, corresponding to four choices of origin and also reflection through a vertical mirror line (Ref. 2). Changing the orientation of all rotors by 90° leads to an equivalent pinwheel state.

TABLE I. Occupation energies $E(9a)$ for galleries as numbered in Fig. 9(a) and similarly for those in Fig. 9(b).

Gallery	E [9(a)]/γ	E [9(b)]/γ
1	−3	3
2	1	−1
3	1	−1
4	1	−1
5	1	−1
6	−3	3
7	1	−1
8	1	−1

phase are zero. This symmetry does not allow a cubic term, since such a term would differentiate two equivalent structures.) The galleries in the cosine pinwheel phase are illustrated in Fig. 9. From the gallery occupation energies listed in Table I one can understand the effect of the cubic term in structure selection. For simplicity, consider first the case when $c_3\gamma$ is positive. Then it is favorable to first fill the galleries labeled 1 and 6 in Fig. 9(a). Note that the sum of all the gallery occupation energies is zero. Accordingly, when less than half the galleries are filled, the structure of Fig. 9(a) is favored. In Fig. 9(b) we see that galleries 1 and 6 have the highest possible energy, so they are the ones which will be filled last. Accordingly, for more than half filling the structure in Fig. 9(b) will be favored. Amazingly, these results are incorporated in the cubic term of Eq. (79).

We now make a rough estimate of the discontinuity in the order parameter for the transition into the commensurate cosine phase, assuming the coefficient w of the cubic term to be small. We have the grand potential in the form

$$\frac{\Omega}{N} = \frac{1}{2}[T - T_c(\mu)][Y_1^2 + Y_2^2 + Y_3^2] + wY_1Y_2Y_3 + u_c[Y_1^2 + Y_2^2 + Y_3^2]^2 + v_c[Y_1^2Y_2^2 + Y_2^2Y_3^2 + Y_1^2Y_3^2] , \quad (83)$$

where the coefficients are

$$w = (81\sqrt{2}/8)c_3\gamma^3(k_BT)^{-2} , \quad (84)$$

$$u_c = \frac{k_BT}{16} + \frac{81c_4\gamma^4}{32(k_BT)^3} , \quad (85)$$

$$v_c = \frac{k_BT}{16} + \frac{81c_4\gamma^4}{8(k_BT)^3} . \quad (86)$$

The result for w is from Eq. (81). The results for u_c and v_c are obtained in analogy with Eqs. (59) and (66). There are no induced fourth-order terms because coupling to zero wave vector or to the herringbone sine modes vanishes: $\phi_c(0) = \phi_s(0) = 0$ and $\phi_s(\mathbf{Q}_A) = 0$. By minimizing the form in Eq. (83) one finds the temperature T_0 for the first-order phase transition into the cosine pinwheel phase as $T_0 = T_c(\mu) + \Delta T$, where $T_c(\mu)$ is given by Eq. (45) and for $\beta = 2$

$$\Delta T = w^2/(54u_c + 18v_c) . \quad (87)$$

Just inside the ordered phase, i.e., for $T \to T_0^-$, the order parameter satisfies

$$|Y_i| = 3\Delta T/|w| . \quad (88)$$

We will compare this result to our numerical results in the next section.

Note that the cubic term in Eqs. (79) and (81) is proportional to c_3 which vanishes for $z = 1$, i.e., for $\langle n_v \rangle = 1/2$. At or near this point, fourth-order terms compete with the above cubic contribution. We will not study this case here.

C. 120° phases

Here we briefly comment on the nature of the higher-order terms at point B in Fig. 4, where the cosine and sine-order parameters are simultaneously critical. At this point, the "root 3" wave vectors, $\mathbf{Q}_{\sqrt{3}}$ and $-\mathbf{Q}_{\sqrt{3}}$ (see Fig. 7) represent the complete star of the critical wave vector. Then $s_y = \sqrt{3}/2$, $c_y = 1/2$, and the analog of Eq. (55) (for the case of two critical wave vectors with complex conjugate amplitudes) becomes

$$\langle E_l(\mathbf{R}) \rangle = \frac{3}{4}\gamma\left[e^{-i\mathbf{Q}_{\sqrt{3}}\cdot\mathbf{R}}(Y + iX) + e^{i\mathbf{Q}_{\sqrt{3}}\cdot\mathbf{R}}(Y^* + iX^*)\right] . \quad (89)$$

In view of Eq. (56), this yields a third-order contribution to Ω of

$$\frac{\delta\Omega^{(3)}}{N} = \frac{27c_3\gamma^3}{32(k_BT)^2}\left[(Y + iX)^3 + (Y^* + iX^*)^3\right] . \quad (90)$$

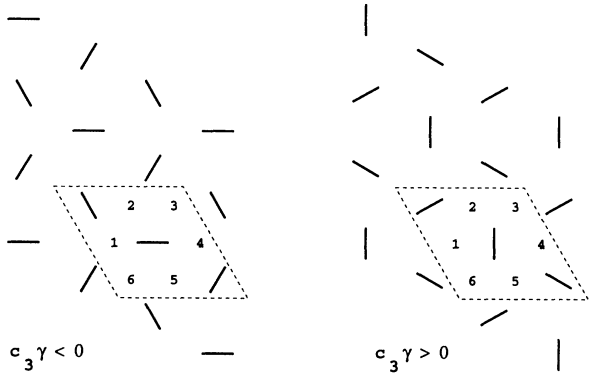

FIG. 11. The two 120° phases associated with the $\sqrt{3}$ wave vectors. (a) Left: the 120° phase which occurs when the gallery occupation probability is greater than 1/2. At low temperature only gallery 1 is unoccupied. (b) Right: the 120° phase which occurs when the gallery occupation probability is less than 1/2. At low temperature only gallery 1 is occupied. Note that the vertical (nearest-neighbor) and horizontal (second-neighbor) directions are *not* equivalent. Also, reflection through a vertical mirror line produces structures equivalent to those shown here.

This term is similar to what one finds for the antiferromagnetic x-y model on a triangular lattice:[20] It is extremized (subject to keeping the quadratic term fixed) by choosing $X = i\sigma Y$, where $\sigma = \pm 1$. Then the phase of Y is restricted to extremize the cubic term. If we set $Y = |Y|e^{-i\phi}$, then

$$\delta\Omega^{(3)} = 27Nc_3\gamma^3|Y|^3\cos(3\phi)/[4(k_BT)^2] . \quad (91)$$

Thus $\cos(3\phi)$ is of unit magnitude and has the same sign as $-c_3\gamma$. The resulting "120°" phases are shown in Fig. 11.

V. PHASE DIAGRAM

The above analysis is not sufficient to construct the phase diagram, because it cannot tell us whether or not a first-order transition to some type of order preempts the instability found from quadratic fluctuations. So it is necessary to supplement the above analysis with some actual evaluations of self-consistent field theory. However, before doing that we establish an exact relation between occupied and unoccupied galleries, similar to particle-hole symmetry in the Hubbard model.

A. Particle-hole symmetry

This general relation relates two phases which are obtained from one another by rotating each rotor through an angle of 90° and interchanging occupied and unoccupied galleries. To develop this relation we set $\theta' = \theta + 90°$, and write

$$\begin{aligned}\mathcal{H}(\{\theta_i\},\{n_v\}) &= \sum_{\langle ij\rangle} V_{ij}(\theta_i,\theta_j) + \sum_v n_v E_v(\{\theta_{v+\delta}\}) \\ &= \sum_{\langle ij\rangle} V_{ij}(\theta_i',\theta_j') + \sum_v n_v[-E_v(\{\theta'_{v+\delta}\})] \\ &= \sum_{\langle ij\rangle} V_{ij}(\theta_i',\theta_j') + \sum_v (1-n_v)E_v(\{\theta'_{v+\delta}\}) \\ &\quad - \sum_v E_v(\{\theta'_{v+\delta}\}) . \end{aligned} \quad (92)$$

By considering a given rotor and summing over its nearest-neighboring shell of galleries, one can show that the last sum in the last line of the above equation vanishes. Therefore the result is

$$\mathcal{H}(\{\theta_i\},\{n_v\}) = \mathcal{H}(\{\theta_i'\},\{n_v'\}) , \quad (93)$$

where $n_v' = 1 - n_v$. In terms of the grand potential we have

$$\Omega(\{\theta_i\},\mu) = \Omega(\{\theta_i'\},-\mu) . \quad (94)$$

This result indicates that as μ passes through zero, the rotors will be rotated through an angle of 90°. For the single wave vector herringbone phases (shown in Fig. 6), this is a symmetry operation, so passing through this point need not correspond to a phase transition. However, for the triple wave vector (HB,c) states and the $\sqrt{3}$ phases, this operation will give rise to a first-order transition, in the former case between the two states shown in Fig. 9, and in the latter case (for the 90° phase) between the two states shown in Fig. 12.

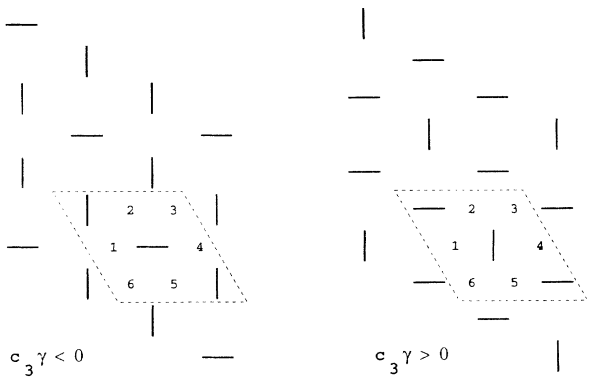

FIG. 12. As in Fig. 11. The two 90° phases at the $\sqrt{3}$ wave vector, in which there are three rotors and six galleries per unit cell (indicated by dashed lines). (a) Left: the 90° phase which occurs when the gallery occupation probability is greater than 1/2. At low temperature only galleries 1 and 4 are unoccupied. (b) Right: the 90° phase which occurs when the gallery occupation probability is less than 1/2. At low temperature only galleries 1 and 4 are occupied.

Another aspect of the symmetry at $\mu = 0$ is that at that point the odd order terms in the Landau expansion vanish. In that case Eq. (11) becomes

$$\begin{aligned}\Omega_v &= \sum_v E_v/2 - k_BT\sum_v \ln\{2\cosh[\langle E_v\rangle/(2k_BT)]\} \\ &= -k_BT\sum_v \ln\{2\cosh[\langle E_v\rangle/(2k_BT)]\} , \end{aligned} \quad (95)$$

which is patently an even function of the order parameters. Since the entropy is also an even function of the order parameters, one sees that for $\mu = 0$ there are no odd order terms in the Landau expansion. (This conclusion holds for all the phases considered in this paper.)

B. Zero-temperature results

We can also use exact calculations of grand potential at zero temperature, since this calculation only requires the energy of a structure characterized by a small number of angles, assuming a small unit cell. The details of the calculations are given in Appendix D of Ref. 13. We have carried out such calculations for structures shown in Figs. 6, 9, and 11–13. The structures which we now consider, but which we have not so far encountered (because they do not occur through an instability of the disordered phase), are (a) the 90° structures (shown in Fig. 12) associated with the root-3 wave vector and (b) the "distorted" structures shown in Fig. 13. The order parameters for the various structures at arbitrary nonzero

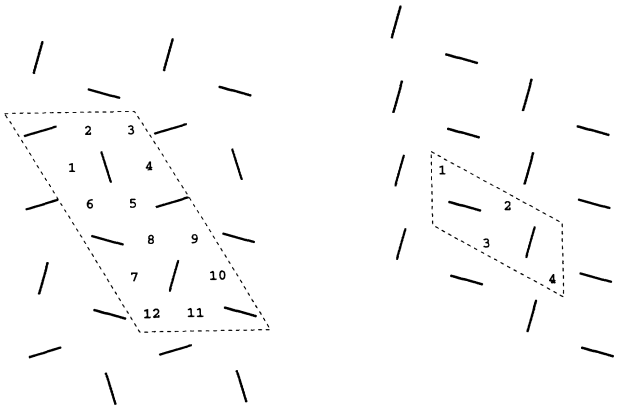

FIG. 13. Distorted phases. (a) Left: the distorted 90° ($d90$) phase. Starting from the 90° phase shown in Fig. 12 (right) all vertically (horizontally) oriented rotors are rotated through an angle of magnitude δ_v (δ_h), with alternating signs, as shown, so that the unit cell is doubled in size. The rotors which were horizontal in Fig. 12 have one order parameter and those which were vertical have another independent order parameter. There are three inequivalent galleries: (1, 4, 7, 10), (2, 5, 9, 12), and (3, 6, 9, 12). (b) Right: the distorted cosine HB (dC) phase in which the two sublattices remain perpendicular to one another but one sublattice makes an angle δ with the HB wave vector. For $\delta = 0$ this phase reduces to the HB,c phase and for $\delta = 45°$ it reduces to the HB,s phase. Both sublattices have the same magnitude order parameter. Galleries 1 and 3 are equivalent as are 2 and 4.

temperature are listed in Table II. To find the energy at zero temperature one sets the magnitude of each (if there are more than one) orientational order parameter equal to unity and sets all the gallery occupation variables to zero except the ones labeled n_1, which is set equal to unity. In the case of the distorted structures, the angle not fixed by symmetry is determined by minimizing the energy. In this way we obtained, in Appendix D of Ref. 13, the results given in Table III. These results were confirmed to very high precision by our numerical work, extrapolated to zero temperature. We emphasize, however, that the "ground states" we find represent only the states of lowest energy within the set of structures considered.

C. Results from self-consistent equations

To obtain actual phase diagrams we allowed the system to relax to the self-consistent equations of mean-field theory as discussed in Appendix C.[13] In so doing, we allowed the system to assume any periodic structure consistent with a unit cell containing 12 rotors. This cell was so constructed (2×6) as to be compatible with both herringbone and $\sqrt{3}$ wave vectors. However, structures with periods too long to fit in such a unit cell were obviously not accessed by this approach. In particular, we had no hope of detecting incommensurate states by this method. As indicated by CM such incommensurate structures are likely to be found only relatively close to the ordering temperature. At low temperature, we would expect lock in to some relatively short-period structure.

With this important caveat, we now turn to a discussion of the numerical results. We will only consider the case $\alpha = -1$. Our numerical results are all for $\beta = 2$, but we will comment on the situation for other values of β. Out calculations were performed for $\gamma = 3$, shown in Fig. 14 and for $\gamma = 4$, shown in Fig. 15. As mentioned above, the phase boundaries at zero temperature agree precisely with our analytic results in Table III. These calculations show that the distorted structures do not occur for large γ. For instance, the results of Table III show that the dC (distorted herringbone cosine) phase only occurs at zero temperature for $\gamma < 2\beta$. Likewise, for $\alpha = -1$ and $\beta = 2$, the $d90$ (distorted $\sqrt{3}$, 90°) phase only occurs at zero temperature for $\gamma < 1 + \sqrt{5} \approx 3.24$.

Most of the transitions shown in Figs. 14 and 15 are of necessity discontinuous ones. The exceptions are (a)

TABLE II. Orientational order parameters and gallery occupation expectation values for various periodic phases.

Phase	Fig.	n_{uc}[a]	Orientational order parameters	$\frac{\langle n_v\rangle_0}{2N}$[b]	n_1[c]	n_2[c]	n_3[c]
HB,s	6(a)	2	$\sigma(45°)$	0			
HB,c	6(b)	2	$\sigma(0) = \sigma(90°)$	1/2	1,3	2,4	
PW,c	9(a)	4	$\sigma(0) = \sigma(60°) = \sigma(120°)$[d]	1/4	1,6	2,3,4,5,7,8	
dC	13(b)	2	$\sigma(-\delta) = \sigma(90° - \delta)$	1/2	1,3	2,4	
120	11(b)	3	$\sigma(0) = \sigma(60°) = \sigma(120°)$	1/6	1	2,4	3,5,6
90	12(b)	3	$\sigma(0) \neq \sigma(90°)$	1/3	1,4	2,3,5,6	
d90	13(a)	6	$\sigma(\pm\phi) \neq \sigma(90° \pm \psi)$	1/3	1,4,7,10	2,5,9,12	3,6,8,11

[a]Number of rotors in the unit cell.
[b]$\langle n_v\rangle_T$ denotes the thermally averaged number of occupied galleries at temperature T. Thus $\langle n_v\rangle_0/(2N)$ is the fraction of galleries occupied at zero temperature.
[c]We list equivalent galleries which all have $\langle n_v\rangle = n_1$, $\langle n_v\rangle = n_2$, and $\langle n_v\rangle = n_3$, with $n_1 \geq n_2 \geq n_3$. See the relevant figure for the labeling of galleries.
[d]One rotor is completely disordered [see Fig. 9(a)].

TABLE III. Zero-temperature energies for selected structures.

Phase	Energy[a]	$\langle n_v\rangle_0/(2n_s)$[b]
HB,s	$-\alpha-\frac{3}{2}\beta$	0
HB,c	$-\alpha+\frac{1}{2}\beta-2\gamma$	1/2
dC[c]	$\mathrm{Min}_c[-\alpha-(3/2)\beta+2\beta c^2-2\gamma c]$	1/2
$d90$[d]	$\frac{2}{3}\mathrm{Min}_c\left[-1-\gamma c+c^2-\sqrt{4-4c^2+\gamma^2}\right]$	1/3
120	$-(3/2)\alpha-(3/4)\beta-\gamma$	1/6
90[e]	$\alpha+\beta/2-2\gamma/3-\lvert 2\alpha+\beta+(2/3)\gamma\rvert$	1/3
PWc[f]	$-[6\alpha+3\beta+3\gamma]/8$	1/4

[a] Min_c means to minimize with respect to c, with $-1\le c\le 1$.
[b] As in Table II.
[c] This phase is undistorted, i.e., it is the HB,c phase, if $c=1$, as happens for $|2\beta/\gamma|<1$.
[d] The energy quoted for this case is for $\alpha=-1$ and $\beta=2$. The more general result obtained in Appendix D of Ref. 13 is $E=\min_c E(c)$, where $3E(c)=-\alpha-3\beta/2-2\gamma c+[4\alpha+3\beta]c^2-R$, where $R^2=(2\alpha+3\beta)^2(1-c^2)+[(6\alpha+3\beta)c+2\gamma]^2$.
[e] For $2\alpha+\beta+(2/3)\gamma>0$ (the case we consider in Figs. 14 and 15), the structure is that of Fig. 12(b). For $2\alpha+\beta+(2/3)\gamma<0$, the structure is that of Fig. 12(a).
[f] This phase, in which there is one disordered rotor [see Fig. 9(a)], does not actually occur at $T=0$.

the transition from the disordered phase to the herringbone sine phase (but including fluctuations causes this transition to become discontinuous[8]), and (b) the transitions from the distorted dC or $d90$ phases, to their undistorted counterparts. In principle the transition from the distorted $d90$ $\sqrt{3}$ structure to the HB,s phase could be continuous, as noted in the caption to Fig. 13. However, since this transition occurs at low temperature, it is not easy to numerically investigate whether or not this transition is in fact continuous.

We established that the transitions of type (b), above, were continuous as follows. In the lower-symmetry phase the rotors tip away from their high-temperature symmetry directions. Consider first the HB,c to dC transition which takes place for μ between about -0.3 and 0, and for near $T=1.5$, as shown in Fig. 14 for $\gamma=3$. If the herringbone vector lies along the x axis, then in the high-temperature phase all rotors have $\langle\cos(2\theta_i)\rangle=\pm\sigma$ and $\langle\sin(2\theta_i)\rangle=0$. In the low-temperature (distorted) phase, shown in Fig. 13, we set $\langle\sin(2\theta_i)\rangle=\pm\eta$. For $\mu=-0.08$, we found that $\eta(T)^2$ was linear in T: For $T=1.50, 1.495, 1.49, 1.485$ and 1.48, we obtained $1000\eta^2=4.54$, 6.14, 7.75, 9.35, and 10.94, respectively. The nearly perfect linearity of these results is an indication of their accuracy. These data establish the characteristic signature of a continuous transition within mean-field theory: $\eta\sim\sqrt{T_c-T}$, with $T_c=1.514$ in this case. A similar analysis was performed for the transition from the 90° to the $d90°$ distorted phase which occurs at $\mu=-2.2$ at $T\approx 0.5$. In the high-temperature phase the angles of the rotors are restricted to either be parallel or perpendicular to nearest-neighbor lattice vectors of the triangular lattice, as shown in Fig. 12. In the low-temperature phase, shown in Fig. 13, a deviation in the rotors away from these symmetry directions devel-

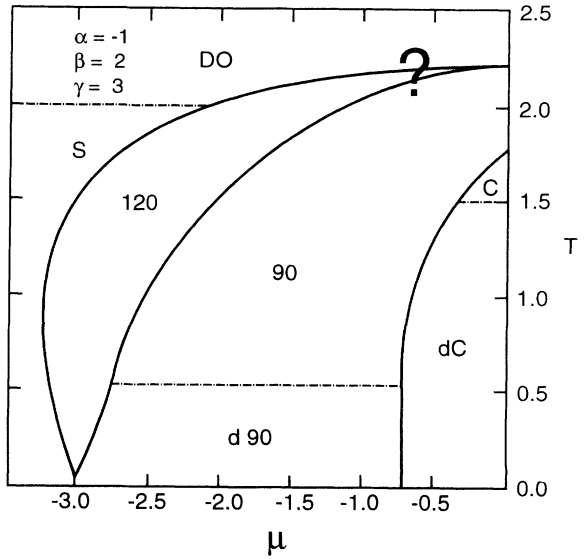

FIG. 14. Results of self-consistent treatment of periodic structures with small unit cells, for $\alpha=-1$, $\beta=3$, and $\gamma=3$. Here DO denotes disordered; S denotes HB,s; 120 (90) denotes the 120° (90°) phase at the $\sqrt{3}$ wave vector, and C denotes the HB,c phase. The dC and $d90$ phase are distorted version of the C and 90 phases (shown in Fig. 13). Continuous phase transitions are indicated by dash-dotted lines. The instability given by Eq. (40) is not shown, but nearly coincides with the phase boundary we show here. The question mark in the upper right part of the phase diagram emphasizes that incommensurate phases (found by CM) are likely to occur in this part of the phase diagram.

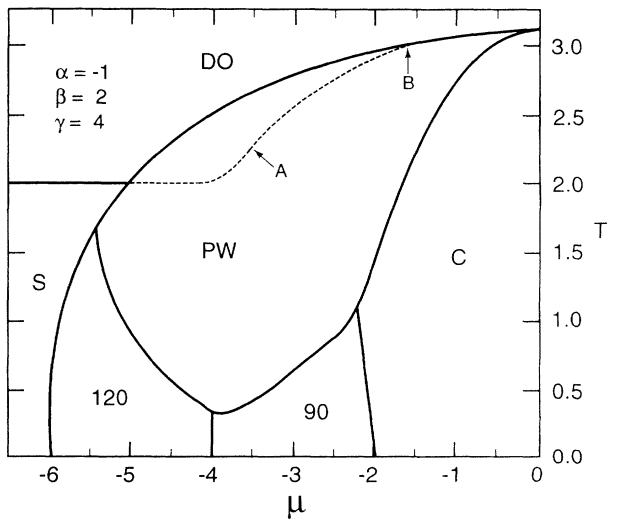

FIG. 15. Results of self-consistent treatment of periodic structures with small unit cells, for $\alpha=-1$, $\beta=3$, and $\gamma=4$, as in Fig. 14. Here PW denotes the cosine pinwheel phase shown in Fig. 9(a). The dashed line is the instability line, given by Eqs. (40), (43), and (45). Points on this line labeled A and B correspond to points A and B in Fig. 4. Near $\mu=0$ this phase diagram becomes uncertain because of the possible occurrence of incommensurate phases, in this case, probably incommensurate cosine phases.

ops. If the axes are properly chosen an order parameter analogous to η in the previous example can be identified and again numerically is found very accurately to vary as $\sqrt{T-T_1}$, where T_1 is the critical temperature for this transition. This characteristic square root behavior indicates a continuous phase transition. (The fact that symmetry consideration alone indicate that these transitions are *allowed* to be continuous does not indicate whether they *actually* are continuous or not. This can only be settled by a quantitative analysis.)

We also performed a test of Landau theory *vis a vis* the first-order transition from the disordered phase into the cosine pinwheel (PWc) phase. For $\alpha=-1$, $\beta=2$, and $\gamma=4$ we collected data at $\mu=-2$. Using the small cell self-consistent equations, we found the disordered phase to minimize the free energy at $T=2.978$. At $T=2.977$ the PWc phase minimizes the free energy and for each of the three ordered rotors in this phase, we found $\langle\cos(2\theta-2\theta_0)\rangle_T=0.226\,67$, where θ_0 is the equilibrium angle of the rotor in question. We checked that this order parameter varied linearly (with temperature) near the transition to exclude categorically the possibility that this transition (at $T_0\approx 2.977$) might be a continuous one. Also for this value of μ we evaluated the instability temperature [see Eq. (45)] to be $T_c(\mu=-2)=2.904$. Now we compare these results to the predictions of Landau theory. For $\gamma=4$, $\mu=-2$, and $T=2.904$ we find that $u_c+(v_c/3)=0.440$ and $w=1.337$, so that Eq. (87) gives $\Delta T=0.075$ which is in good agreement with our numerical determination $\Delta T=2.977-2.904=0.073$. Likewise, the Landau expansion prediction of Eq. (88) for the order parameter at $T=T_0^-$ gives $|Y_i|=3(2.977-2.904)/1.337\approx 0.17$. From Eq. (82) one sees that for the ordered rotors in the PWc phase, $\langle\cos(2\theta-2\theta_0)\rangle_T=\sqrt{2}|Y_i|$. Our direct numerical solution for this average thus yields $|Y_i|=0.226\,67/\sqrt{2}\approx 0.16$, in reasonable agreement with the above estimate based on the Landau expansion. In this case, therefore, the Landau expansion carried up to order Y^4 satisfactorily describes the first-order transition into the HBc phase.

Next some general comments are in order. The most obvious aspect of these phase diagrams is that one sees a progression of structures which progressively accommodate more and more occupied galleries as μ is increased. This was noted in a general way by CM and we confirm this. A surprising aspect of these results is that these phase diagrams could not have been predicted on the basis of the lowest-order terms in the Landau expansion. This is why our results do not look very similar to those of CM who used Landau theory together with a few zero-temperature calculations to construct a phase diagram. Landau theory indicates that as the chemical potential is increased, the herringbone sine phase is followed by an incommensurate sine phase. To assess the likelihood that this phase actually does appear, we have shown on the phase diagrams the instability temperature given with Landau theory for the I,s phase. To start, consider Fig. 15, for $\gamma=4$. First, recall the results of Sec. IV A: the I,s phases do *not* support a cubic term in the Landau expansion. Also over a small part of the range, the fourth-order term, u_s, shown in Fig. 8, is positive. In that case we expect the instability towards forming an incommensurate phase to occur where the quadratic term is unstable. (Although Fig. 8 is for $\gamma=3$, this observation also applies for $\gamma=4$.) Since, as the temperature is lowered, the PW,c phase has already condensed before this instability is reached, it seems unlikely that the I,s forms, at least for μ sufficiently negative. Near $\mu=0$, it is likely that incommensurate phases do exist, but judging from the location of the instability line for the I,s and I,c phases, the incommensurate cosine phases is the one most likely to exist. For the I,c phases, a triple wave vector state is almost guaranteed by the existence of a cubic term, as discussed in Sec. IV D.

For $\gamma=3$, the situation is less clear. It seems quite possible that for temperatures above, say, 1.5, the phase diagram in Fig. 14 is quite wrong and that incommensurate phases do occur. However, in contrast to the CM phase diagram, it seems unlikely that the single wave vector or striped phase occurs, since v_s of Eq. (74) shown in Fig. 8 is normally negative. The question mark near $\mu=0$ is inserted in Fig. 14 to emphasize this uncertainty.

D. Multicritical points

We now very briefly discuss special points within this model. For simplicity, we restrict the discussion to $\alpha=-1$. The multicritical points where three phases coexist are so numerous that we will restrict ourselves to the more piquant aspects of the phase diagrams.

The most striking multicritical point might be that shown in Fig. 4 at $\beta=4/3$ and $x=1/6$. At this point, as we have already noted, the fluctuation matrix of Eq. (24) is totally independent of wave vector. (In that sense it may be called an "infinite degeneracy" point.) Here the instability temperature, T_0 is unity. To reach this point ($\beta=4/3$, $x=1/6$, $T=1$), one must satisfy Eq. (28) so that

$$16\cosh^2[\mu/(2k_BT)]=6\gamma^2\,. \tag{96}$$

By taking $\mu=0$ (and therefore $\gamma=\sqrt{8/3}$), we eliminate cubic terms in Landau theory and we may then indeed have a situation similar to that of the *kagomé* antiferromagnet,[14] where wave vector selection occurs through thermal fluctuations. (In that case a $\sqrt{3}$ phase was favored.)

A lower-order multicritical point (noted by CM) occurs when the unstable wave vector is the $\sqrt{3}$ wave vector. As indicated Fig. 4 and Sec. III, this requires $x=\beta/8$ and the instability temperature, according to Eq. (40), is $T=(15\beta/8)-(3/2)$. Combining this with Eq. (28), we see that if $\mu=0$, then

$$\beta=\frac{2}{5}+\frac{2}{15}\sqrt{9+15\gamma^2} \tag{97}$$

and this will apply as long as $\gamma>\sqrt{8/3}$. This point occurs in Fig. 4, since Eq. (97) is satisfied by $\beta=2$ and $\gamma=3$. Here we have again put $\mu=0$ to enhance the

chance that the transition is a continuous one. (In this case, $x = 1/4$, which is point B in Fig. 4.) Unfortunately, our numerical methods are not ideally suited to studying such a multicritical point, especially since it is vital to test for the occurrence of incommensurate states. (If $\gamma = \sqrt{8/3}$, this point becomes the infinite degeneracy point considered above.)

Yet another multicritical point that has some interest is that which occurs in Fig. 14 (for $\gamma = 3$) where the (HB,s), $d90$, and 120° phases coexist. This point is *not* at zero temperature, as one can verify using the results given in Table III. However, if the parameters are suitably adjusted we can obtain a similar, but simpler, multicritical at zero temperature at which the HB,s, the 120°, and the 90° phases coexist. From the results in Table III one can see that the 90° phase is undistorted providing $\gamma > \gamma_c$, where

$$\gamma_c = -\alpha + [5\alpha^2 + 9\alpha\beta + (9\beta^2/2)]^{1/2} . \tag{98}$$

(To determine γ_c, set $\partial E/\partial c|_{c=1} = 0$ for the $d90$ phase.) We assume that γ is larger than γ_c and we set $\alpha = -1$. Then from Table III we obtain the potentials for the various phases: $\Omega_{\mathrm{HB},s} = 1 - (3/2)\beta$, $\Omega_{90} = 1 - (\beta/2) - (4\gamma/3) - (2\mu/3)$, and $\Omega_{120} = (3/2) - (3\beta/4) - \gamma - (\mu/3)$. The three potentials are simultaneously equal at a critical value of μ (denoted μ_c) providing

$$\beta = (4\gamma/3) - 2 , \tag{99}$$

in which case $\mu_c = -3$. But for this point to actually occur, the $d90$ phase must not intervene. This requires that $\gamma > \gamma_c$ and that Eq. (99) be satisfied. These conditions that the multicritical point where the HB,s, 120°, and 90° phases coexist at $T = 0$ require that $2 < \gamma < 20/7$. (Thus this multicritical point does not quite occur in Fig. 14.) Near this multicritical point the 120° phase remains stable in a wedgelike region ending at the point $\mu = -3$ and $T = 0$ on the phase diagram. In this case, a spin-wave-type calculation could enable one to draw the phase diagram, as was done in a similar situation in Ref. 8.

There are further interesting points on the $\mu = 0$ axis, where the particle-hole symmetry relation indicates the existence of multicritical points. We will not explore these here.

VI. SUMMARY

In this paper we have studied the model proposed by Choi and Mele[7] (CM) for alkali-metal doping of crystalline polyacetylene. In this model the anisotropic interaction between polymer chains (characterized by a dipolar coupling constant α and a quadrupolar coupling constant β) is supplemented by a steric interaction between polymer chains and dopants (with coupling constant γ) such that the dopants tend to form triangular galleries. In this model, the polyacetylene chains are replaced by rotors on a two-dimensional lattice.

We treated the above model by a variety of numerical and analytic techniques, mostly based on mean-field theory. We briefly summarize conclusions to be drawn from this work.

(1) The main conclusion of Choi and Mele,[7] namely that doping causes frustration which is relieved by structural modification, is verified.

(2) As the doping is increased, we find an unexpectedly rich sequence of phases involving compositional and orientation order. For instance, in the phase diagrams of Figs. 14 and 15, for two different values in the parameter space α-β-γ, we find seven distinct ordered phases.

(3) As might be expected for competing interactions, most of the transitions are discontinuous. Changing the number of low-energy galleries is not usually done in a continuous fashion. However, distortions from ideal structures were identified. Such distortions were shown numerically to give rise to continuous phase transitions, e.g., see Fig. 14 at $\mu = -0.4$ and $T \approx 1.5$ and also at $\mu = -2$ and $T \approx 0.5$.

(4) An exact symmetry relation, similar to the usual particle-hole symmetry in the Hubbard model, was identified for the first time. This relation relates the grand potential at chemical potential (of dopants) μ to a transformed state at chemical potential $-\mu$ in which all rotors are rotated through 90°. In some situations this relation implies the existence of a phase transition at $\mu = 0$.

(5) A reanalysis of higher-order terms in the Landau expansion shows that the herringbone sine phases (both commensurate and incommensurate) do not support terms which are third order in the order parameter. This fact, together with our numerical implementation of mean-field theory, shown in Figs. 14 and 15, makes it unlikely that the incommensurate sine phase occurs. In any event since the relevant fourth-order term (v_s in Fig. 8) in the Landau expansion is negative, if such a phase does occur, it is very likely to occur with simultaneous condensation at all wave vectors in the star of the unstable wave vector.

(6) The incommensurate cosine ordered phases do support third-order terms in the Landau expansion. These make it almost certain that one has simultaneous condensation of all wave vectors in the star. They also make our numerical determination of the phase diagram very uncertain, and, in fact, quite likely to be wrong. Thus, it seems likely that such incommensurate states *do* occur, although our analysis of them is not quantitative. (Qualitatively speaking, the cosine phase have galleries more adaptive to dopants than do the sine phase, as can be seen from Fig. 6.)

(7) A very simple argument, given in Eq. (95), shows that for the special case $\mu = 0$ (where the galleries are essentially half filled), there are no odd order terms in the Landau expansion.

(8) A number of potentially interesting multicritical points were identified in this model, as discussed in Sec. V D. For instance, at one of these the generalized susceptibility matrix is independent of wave vector. This "infinite" degeneracy is even more severe than in the case of the *kagomé* antiferromagnet[14] because here all branches are the susceptibility are wave vector independent. There is also a zero-temperature multicritical point whose degeneracy is lifted by thermal fluctuations as in

other anisotropic rotor models.[8] Finally, the multicritical point (identified previously by CM) where sine and cosine ordering occur simultaneously is discussed. The point they mentioned has a further degree of degeneracy because it occurs at $\mu = 0$, where odd order terms in the Landau expansion are not allowed.

(9) We also point out that although this model is physically attractive for low doping, it probably needs to modified for higher doping. On the triangular lattice neighboring galleries form a honeycomb lattice with adjacent galleries quite close together. Probably some short-range repulsion should be included to prevent adjacent galleries from being occupied. (Such an interaction would compete with the removal of frustration which the current model attributes to such a configuration.)

ACKNOWLEDGMENTS

We acknowledge helpful conversations with T. C. Lubensky and E. J. Mele. This work was supported in part by the National Science Foundation under Grant No. DMR91-22784. We also acknowledge partial support from the National Science Foundation under the MRL program, Grant No. DMR88-19885. Some of the computations were supported by a grant from the Research Foundation of the University of Pennsylvania.

[1] C. R. Fincher, Jr., C. E. Chen, A. J. Heeger, A. G. McDiarmid, and J. B. Hastings, Phys. Rev. Lett. **48**, 100 (1982).
[2] A. B. Harris and A. J. Berlinsky, Can. J. Phys. **57**, 1852 (1979).
[3] H.-Y. Choi, A. B. Harris, and E. J. Mele, Phys. Rev. B **40**, 3766 (1989).
[4] J. Ma, J. E. Fischer, E. M. Scherr, A. G. MacDiarmid, M. E. Josefowicz, A. J. Epstein, C. Mathis, B. Francois, N. Coustel, and P. Bernier, Phys. Rev. B **44**, 11 609 (1991).
[5] Alkali-metal-doped polyacetylene: M. Winokur, Y. B. Moon, A. J. Heeger, J. Barker, D. C. Bott, and H. Shirakawa, Phys. Rev. Lett. **58**, 2329 (1987).
[6] D. Djurado, J. E. Fischer, P. A. Heiney, J. Ma, N. Coustel, and P. Bernier, Synth. Met. **34**, 683 (1989); P. A. Heiney, J. E. Fischer, D. Djurado, J. Ma, D. Chen, M. J. Winokur, N. Coustel, P. Bernier, and F. E. Karasz, Phys. Rev. B **44**, 2507 (1991); J. E. Fischer, P. A. Heiney, and J. Ma, Synth. Met. **41-43**, 33 (1991).
[7] Han-Yong Choi and E. J. Mele, Phys. Rev. B **40**, 3439 (1989).
[8] A. B. Harris, O. G. Mouritsen, and A. J. Berlinsky, Can. J. Phys. **62**, 915 (1984).
[9] H.-D. You, S. C. Fain, Jr., S. Satija, and L. Passell, Phys. Rev. Lett. **56**, 244 (1986).
[10] D. E. Moncton, J. D. Axe, and F. J. DiSalvo, Phys. Rev. Lett. **34**, 734 (1975).
[11] W. McMillan, Phys. Rev. B **12**, 1187 (1975).
[12] For a review, see P. Bak, Rep. Prog. Phys. **45**, 587 (1982).
[13] See AIP document no. PAPS PRBMD-50-12 441-13 for 13 pages of Appendices A (Location of Critical Points), B (Induced Quartic Terms), C (Mean Field Theory for Commensurate Structures), and D (Zero Temperature Results). Order by PAPS number and journal reference from American Institute of Physics, Physics Auxiliary Publication Service, 500 Sunnyside Boulevard, Woodbury, New York 11797-2999. The price is $1.50 for each microfiche (60 pages) or $5.00 for photocopies of up to 30 pages, and $0.15 for each additional page over 30 pages. Make checks payable to the American Institute of Physics. Airmail additional.
[14] A. B. Harris, C. Kallin, and A. J. Berlinsky, Phys. Rev. B **45**, 2899 (1992).
[15] J. Villain, R. Bidaux, J. P. Carton, and R. Conte, J. Phys. (Paris) **4**, 1263 (1980).
[16] C. L. Henley, Phys. Rev. Lett. **62**, 2056 (1989).
[17] J. Frenkel and T. Kontorova, Phys. Z. Sowjetunion **13**, 1 (1938); F. C. Frank and J. H. van der Merwe, Proc. R. Soc. London **198**, 205 (1949); S. Aubry, in *Lecture Notes in Mathematics*, edited by D. Chudnovsky and G. Chudnovsky (Springer, Berlin, 1982), Vol. 925, p. 221.
[18] M. E. Fisher and W. Selke, Phys. Rev. Lett. **44**, 1502 (1980); P. Bak, Rep. Prog. Phys. **45**, 587 (1982).
[19] A. B. Harris, E. Rastelli, and A. Tassi, J. Appl. Phys. **67**, 5445 (1990); A. B. Harris, *ibid.* **69**, 6173 (1991).
[20] H. Kawamura, J. Appl. Phys. **61**, 3590 (1987).